Recruitment of *GRASSY TILLERS1 (GT1)* and *RAMOSA3 (RA3)* into distinct genetic networks in the evolution of grass morphology

Amber E. de Neve[1,2*], Olivia A. Kelly[1], Terice Kelly[1,3], Samuel Leiboff[2], Madelaine E. Bartlett[1,3*]

[1]Department of Biology, University of Massachusetts; Amherst, MA, USA.
[2]Oregon State University; Corvallis, Oregon, USA.
[3]Sainsbury Laboratory Cambridge University (SLCU); Cambridge, UK.
*communicating authors

Abstract: Changes in form are driven by the differential, context-dependent regulation of pleiotropic genes. How genetic pleiotropy itself emerges, however, remains unclear. The maize genes *GRASSY TILLERS1* (*GT1*) and *RAMOSA3* (*RA3*) are required for axillary meristem suppression, a deeply conserved trait across angiosperms, and for floral organ suppression, a trait which evolved within the grass family. To determine how these pleiotropic functions are regulated, we first established a high-throughput method for quantitative phenotyping of grass flowers. Using this method, we show that distinct environmental mechanisms regulate axillary meristem versus floral organ suppression. In line with these differences, we find upstream regulation of *GT1* and *RA3* has diverged, consistent with their redeployment in flowers. Our results show that, rather than wholesale adoption of genetic networks, developmental genes can retain ancient functions *and* be recruited into other programs in the evolution of form, thereby increasing genetic pleiotropy.

Main Text: Rather than generating new proteins through coding sequence changes, morphological evolution often arises from changes in when and where conserved proteins are expressed (King & Wilson, 1975; Carroll, 2005). Mutations that impact gene expression instead of protein structure can generate evolutionary novelty while minimizing harmful side effects, thus reducing the risk of negative mutational pleiotropy from drastic changes to protein coding sequences (Prud'homme *et al.*, 2007). Pleiotropy, the influence of a single locus on multiple traits, exists in two forms: mutational pleiotropy, where single base pair substitutions, insertions, or deletions affect multiple genetic functions; and genetic pleiotropy, in which null mutations abolish all functions of a gene (Stearns, 2010; Zhang, 2023). While both mutational and genetic pleiotropy can be positive (or adaptive) for evolution (Foster *et al.*, 2004; Kostyun *et al.*, 2019; Hämälä *et al.*, 2020), negative (or antagonistic) pleiotropy occurs when evolution is constrained due to phenotypic effects that both increase and decrease fitness (Zhang, 2023). As the number and complexity of traits influenced by pleiotropy increase, beneficial mutations become less likely, as positive effects get diluted by unwanted negative side effects on other traits (Orr, 2000; Welch & Waxman, 2003). This layered complexity often obscures the origins of pleiotropy, which remain difficult to pinpoint.

Pleiotropy may emerge from the same genetic modules being redeployed to shape morphology. For example, parts of the genetic program regulating lateral branch initiation in maize are recruited

to promote the growth of the leaf ligule, a specialized hinge structure at the sheath-blade boundary (Johnston *et al.*, 2014; Bertolini *et al.*, 2025). While in this case module redeployment promotes growth, in other contexts modules can be co-opted to suppress it (Klein *et al.*, 2022).

In maize, two pleiotropic genes involved in growth suppression are *GRASSY TILLERS1* (*GT1*) and *RAMOSA3* (*RA3*) (Satoh-Nagasawa *et al.*, 2006; Whipple *et al.*, 2011; Klein *et al.*, 2022). *GT1* controls selective pistil suppression in maize tassel flowers, a process that is essential to the development of unisexual staminate flowers (Whipple *et al.*, 2011). Unisexual flowers in the maize tassel initiate both stamen and pistil primordia, then pistil primordia undergo cell death leaving behind only the stamens (Calderon-Urrea & Dellaporta, 1999). Besides its role in flower development, *GT1* is also an important regulator of tillering; *gt1* mutants have pistils in tassel florets, as well as additional tiller branches and husk leaves (Whipple *et al.*, 2011). *RA3* also affects both branching and floral development and encodes a trehalose-6-phosphate (Tre6P) phosphatase (Satoh-Nagasawa *et al.*, 2006; Klein *et al.*, 2022). Notably, double *gt1;ra3* mutants have increased tiller branching compared to *gt1* alone, and fully derepressed pistils in both tassels and ears (Klein *et al.*, 2022). Both GT1 and Tre6P phosphatases like RA3 have ancient roles in regulating tiller suppression. *GT1* homologs suppress tiller branching in brachypodium, rice, and arabidopsis (González-Grandío *et al.*, 2017; Kumar *et al.*, 2021; Gallagher *et al.*, 2023; Sánchez-Gerschon *et al.*, 2024). Similarly, Tre6P phosphatases like RA3 regulate branching across species: increased Tre6P phosphatase expression decreases branching in the arabidopsis vasculature (Fichtner *et al.*, 2021), and Tre6P influences branch bud outgrowth initiation in garden pea (Fichtner *et al.*, 2017). Together, *GT1* and *RA3* demonstrate how conserved modules can shape plant form, through their effects on both floral development and tillering.

The evolutionary history of pistil suppression versus tiller suppression is known. Growth suppression of lateral vegetative buds (including grass tillers) is a conserved trait in the angiosperms (Takeda *et al.*, 2003; Aguilar-Martínez *et al.*, 2007; Martín-Trillo *et al.*, 2011; Dixon *et al.*, 2018), while growth suppression of floral organs is derived. Programmed cell death of pistils likely emerged in a lineage leading to the Andropogoneae, the tribe to which maize belongs (Le Roux & Kellogg, 1999). Because these two suppression phenotypes occur within the same organism, regulated by the same genes, maize *gt1* and *ra3* mutants represent an ideal system for dissecting the genetics of tiller and pistil suppression.

In tillering, environmental signals, particularly light and sugar availability, play critical roles in regulating branch suppression (Doust, 2007; Barbier *et al.*, 2015b,a; Demotes-Mainard *et al.*, 2016; Khangura *et al.*, 2020; Patil *et al.*, 2022), but environmental effects on pistil suppression are less clear. *TEOSINTE BRANCHED1 (TB1)* integrates environmental signals to suppress tillering (Doebley *et al.*, 1995; Kebrom *et al.*, 2006). *TB1* homolog expression is induced by shade in sorghum and arabidopsis (Kebrom *et al.*, 2006; González-Grandío *et al.*, 2013), and *TB1* in pea plants is downregulated when bud growth is activated by sucrose (Mason *et al.*, 2014). Notably,

GT1 is a downstream target of TB1 in maize, and TB1 binding peaks are located near *RA3*, which is also downregulated in *tb1* mutants (Dong *et al.*, 2019). *GT1* homolog expression in tillers is induced by shade through TB1 homologs in maize and arabidopsis (Whipple *et al.*, 2011; González-Grandío *et al.*, 2017). The TB1-*GT1* interaction is deeply conserved (González-Grandío *et al.*, 2017), as is environmental plasticity of branching (Rameau *et al.*, 2014; Luo *et al.*, 2021). Environmental conditions can also affect pistil suppression (Nuccio *et al.*, 2015; Qian *et al.*, 2025), but whether the same stressors and upstream regulators as in tillering are involved is unknown.

To assess whether TB1 and environmental signals are upstream of pistil suppression as they are in tillers, we developed a sensitive, high-throughput method that can identify subtle morphological changes in pistils. By examining the impact of defoliation and *tb1* mutant combinations on pistil development, we uncover how novel pleiotropies emerge.

X-ray imaging paired with automated segmentation captures pistil shape data at scale

Measuring maize pistils has been difficult, because each pistil needed to be dissected out of the spikelet (Klein *et al.*, 2022). To address this problem and to investigate the effects of the environment on sporophytic sex determination in maize, we developed a method that combines x-ray imaging and machine learning-based segmentation to measure pistils. We grew maize plants and collected the lowest tassel branch when the anthers emerged from the spikelets and prepared them for x-ray CT (Computed Tomography; Fig. 1a). We chose this collection point 1) to standardize inflorescence maturity, and 2) when the anthers are outside of the spikelet, pistils are clearer on the x-ray image. Because the pistil tissue has high density compared to the surrounding spikelet and branch tissue, the pistils absorb more x-rays and are distinguishable as dark circles in images (Fig. 1b). Instead of reconstructing full 3D volumes, we collected 2D x-ray scans from a reduced number of angles. This approach not only reduced scan time (<5 minutes per tassel branch), but also produced higher-quality images for CNN segmentation than 3D reconstructions, enabling more accurate detection of pistils.

Next, we trained a Mask-RCNN (Region-based Convolutional Neural Network) model to automatically measure pistils from the x-ray images (He *et al.*, 2017). Mask-RCNN models can detect objects in an image and generate segmentation masks of those objects (Fig. 1c). To train the model, we first generated a training data set of 664 x-ray images, including maize mutants with defects in tassel pistil repression and samples of *Setaria viridis* (setaria), a grass where pistils are not repressed under normal conditions (Supplementary Table 1). By incorporating setaria, we built an evolutionarily informed model with enhanced applicability across grasses. We validated the performance of the model (Supplementary Fig. 1; Supplementary Tables 2-3), and determined that applying a confidence threshold of 0.82 maximized the precision (fraction of correct predictions out of all predictions) and recall (fraction of correctly identified positives out of all positives) (Rainio *et al.*, 2024) of high overlap predictions (Supplementary Fig. 1). At the 0.82 confidence threshold, the median Intersection over Union (IoU), a measure of overlap between predicted and

ground truth segmentations, was 0.83 (IQR = 0.73 - 0.89), indicating high accuracy for most predicted pistil segmentations (Supplementary Fig. 1). The model achieved an average precision (AP) of 0.96 at an IoU threshold of 0.50 (AP_{50}), and a mean average precision (mAP) of 0.70 across IoU thresholds from 0.50 to 0.95 in 0.05 increments (Supplementary Fig. 1). Importantly, the model generalized across multiple genotypes, developmental stages, and species, indicating that we built a robust tool for quantifying pistil morphology in grasses.

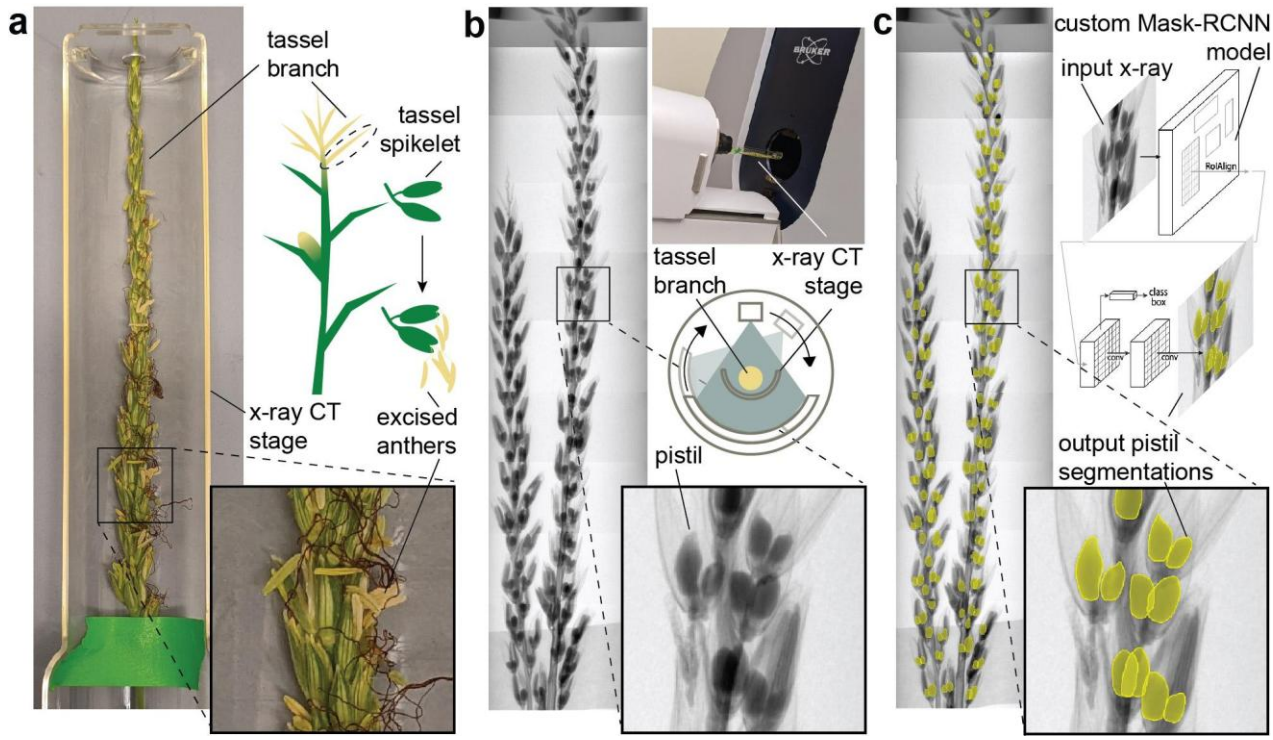

Figure 1. X-ray imaging and automated segmentation quantifies grass floral morphology. a) The bottom tassel branch of a maize plant is collected when anthers are fully emerged from spikelets, and secured to the x-ray CT stage. Ex. *gt1;ra3* maize plant. b) The branch is loaded horizontally into the x-ray CT machine and scans are collected along the length of the sample. Individual scans stitched into whole tassel images. c) Scans are processed by a custom trained Mask-RCNN model to segment pistils (diagram adapted from He et al. 2017), and data from masks are used in subsequent statistical analysis.

Mutant pistils are morphologically varied, and pistil size is affected by spikelet and flower position on the tassel branch

We first used our new method to characterize morphological variability in maize mutants. Floral morphological traits vary along inflorescence axes (Diggle, 1995; Egger & Walbot, 2015).To determine how pistil morphology changed along tassel branches in maize, we assessed the distal-proximal position of pistils on tassel branches. All tassel branch lengths were normalized to 1, and pistil position ranged between 0 at the base - 1 at the tip (Fig. 2a). We quantified pistil presence/absence along branch axes in both *gt1* and *gt1;ra3* mutants. Ectopic derepressed pistils

were present along the whole tassel branch for both genotypes, with fewer pistils found in the top 10% of the branches (Fig. 2b). *gt1* mutants often had just one visible derepressed pistil per spikelet compared to *gt1;ra3* mutants which most often had two clearly visible pistils per spikelet (Fig. 2a,b). Along with fewer pistils, *gt1* tassel branches had fewer total spikelets per branch than *gt1;ra3* (Fig. 2b), likely due to a difference in branch length.

Next, using just the *gt1;ra3* dataset, we quantified pistil size along branches. Pistils at the base of tassel branches were larger than those at the top (base pistils = 0.106 $cm^2 \pm 0.002$; top pistils = 0.084 $cm^2 \pm 0.004$) (Fig. 2c). This is reminiscent of *Ranunculus, Solanum* and orchid species, where distal flowers are smaller than proximal flowers on branches, and some distal flowers are unable to set fruit (Diggle, 1995; Miller & Diggle, 2003; Diggle & Miller, 2004). Along with positional variability across tassel branches, we also found variation in pistil size within spikelets (Fig. 2d,e). Tassel spikelets have two staminate flowers with suppressed pistils, whereas in *gt1;ra3* plants both pistils develop (Klein *et al.*, 2022). To measure differences at the spikelet level, we isolated all pistil pairs (see Methods). One pistil of the pair was on average ~25% smaller than the other (pistil 1 = 0.114 $cm^2 \pm 0.002$; pistil 2 = 0.083 $cm^2 \pm 0.002$) (Fig. 2d,e). This is consistent with previous data showing maize upper floret anthers are roughly twice the size of the lower floret anthers within a spikelet at any point on the tassel (Egger & Walbot, 2015). The upper flower is larger and develops about a day ahead of the lower flower, and genes are differentially expressed between the two floret types (Yang *et al.*, 2022), indicating upper and lower flowers may have developmental differences.

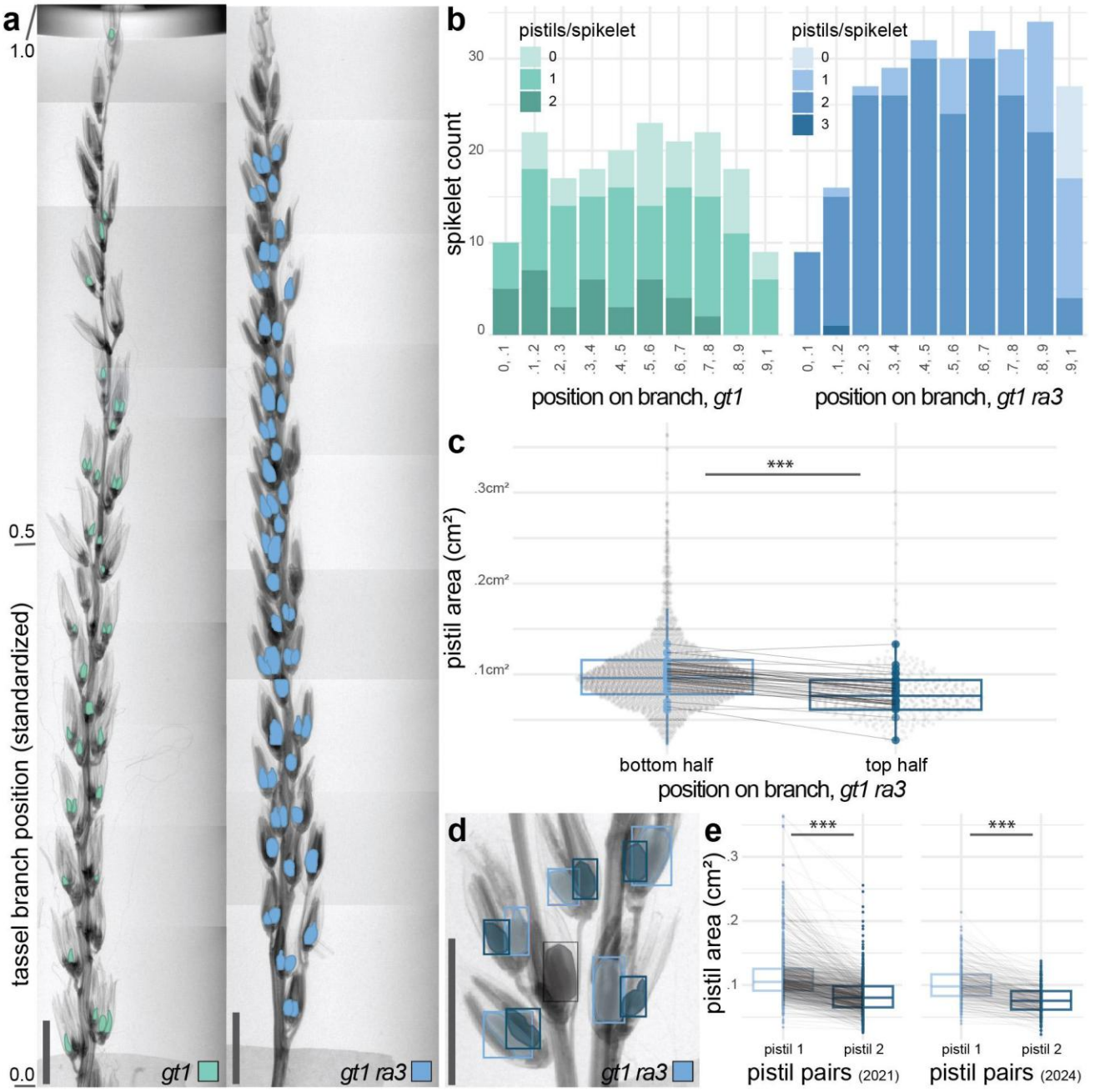

Figure 2. Pistil size changes by branch position. a) Examples of *gt1* and *gt1;ra3* tassel branch x-rays, showing pistil detection masks. The position of pistils on the tassel branch is standardized for each branch, with 0 being the base and 1.0 being the top. Scale bars = 1.9 cm. b) Pistil presence/absence by tassel branch position. Pistils per spikelet for *gt1* and *gt1;ra3* plants. 5 plants measured per genotype (see Methods). c) Pistil area by tassel branch position. *gt1;ra3* tassel branches, bottom halves compared to top halves. Large dots represent the mean pistil area for the branch half, lines connect the same branch. Linear mixed model, pistil area ~ branch position (bottom/top) * block + (1 | plant). Estimated marginal means, $p < .05$, ***. d) Example of pistil spikelet pair detections - light blue, larger of pair; dark blue, smaller of pair; black, filtered (not part of a detection pair). e) *gt1;ra3* pistil pair size comparison within spikelets. Lines connect the pistil pairs, split by year. Student's t-test; $p < .05$, ***.

Because our method captures the outlines of pistils, we could also measure how shape differs across genotypes. We assayed various shape metrics, including elliptical Fourier shape descriptors (Supplementary Fig. 2b), which revealed phenotypes in *gt1;ra3* and *tb1;gt1;ra3*, including rare instances of triple pistils within spikelets and pistils with abnormal morphology (Supplementary Fig. 2c). Upon closer inspection of those flowers with abnormal pistil morphology, likely nucellus tissue and an additional membrane (possibly an ovule integument) were overgrown and protruding out of the outer carpels, which were not fully fused (Supplementary Fig. 2d). This means the chalaza, the ovule-producing meristem (Rudall, 1997; Gross-Hardt *et al.*, 2002), is likely affected in these mutants.

Defoliation affects pistil and branch suppression differently

We noticed a small but significant difference in pistil size in *gt1;ra3* double mutants between years (2021 *gt1;ra3* = 0.101 cm^2 ± 0.002; 2024 *gt1;ra3* = 0.091 cm^2 ± 0.002), suggesting that pistil development is environmentally sensitive (Fig 2c,e), consistent with findings in the ear, the axillary inflorescence of maize (Setter *et al.*, 2001; Gustin *et al.*, 2018). Given that tillering is so sensitive to the environment (Tetio-Kagho & Gardner, 1988; Doebley *et al.*, 1995), and given that this environmental sensitivity feeds through *TB1 (Whipple et al., 2011; González-Grandío et al., 2017)*, we wondered if environmental regulation of tiller and pistil development was similar. To assess this, we defoliated *gt1;ra3* plants during development, a treatment known to decrease tillering in maize, likely because of sugar deprivation (Kebrom *et al.*, 2010; Kebrom & Mullet, 2015).

If the environmental sensitivity of pistil suppression and tillering acted through the same pathways, we expect reduced pistil growth in tassels alongside reduced branching. While defoliation decreased tillering as expected (no treatment = 1.08 ± 0.152; defoliated = 0.673 ± 0.128; n = 37) (Fig. 3b), and decreased inflorescence branching (no treatment = 7.11 ± 0.62; defoliated = 5.06 ± 0.57; n = 37) (Fig. 3a), pistil size and shape were not significantly different between defoliated and untreated plants (no treatment = 0.100 cm^2 ± 0.001; defoliated = 0.098 cm^2 ± 0.002; tassel n = 37; no treatment pistil n = 2892; defoliated pistil n = 1558) (Fig. 3c and Supplementary Fig. 3). Instead, pistil size and shape stayed the same between treatments. This result was remarkably consistent across two experimental replicates, over two field seasons. Thus, pistils in *gt1;ra3* tassels are resilient to sugar deprivation under conditions that decrease the activity of other branching axes. One possibility is that TB1 or other upstream regulators feed only through *GT1* and *RA3* in environmentally mediated pistil suppression, explaining the absence of a pistil phenotype in *gt1;ra3* mutants. Alternatively, pistil and branch suppression may respond differently to defoliation and upstream regulation of suppression has diverged. In either case, these results indicate that suppression is controlled differently in pistils versus branches.

The regulation of *GT1* by TB1 is distinct between tillers and pistils

In addition to sugar, light is a major regulator of tiller suppression, acting upstream of TEOSINTE BRANCHED1 (TB1) to promote tiller outgrowth in shade through differential regulation of its downstream target *GT1* (Tetio-Kagho & Gardner, 1988; Doebley *et al.*, 1995; Kebrom *et al.*, 2006; Whipple *et al.*, 2011; Dong *et al.*, 2017, 2019). The TCP family to which *TB1* belongs also has roles in floral organ suppression (Luo *et al.*, 1996; Yant *et al.*, 2015; Jiao *et al.*, 2018), raising the possibility that *TB1* could contribute to pistil suppression, perhaps through a similar TB1-*GT1* pathway. However, pistil suppression in tassels is normal in *tb1* single mutants (Hubbard *et al.*, 2002), suggesting that other factors could be compensating for the loss of TB1 in this context. We therefore tested if *tb1* affects suppression in different sensitized mutant backgrounds, including *tb1;ra3* double mutants and the *tb1;gt1;ra3* triple.

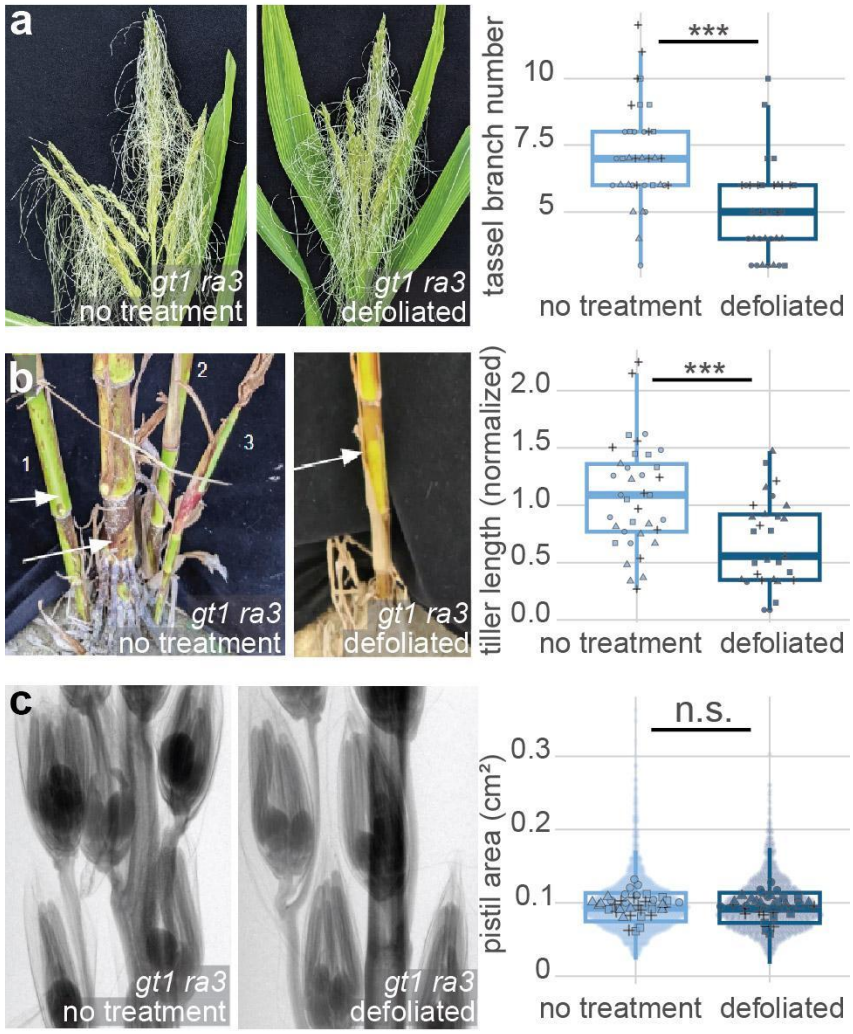

Figure 3. Defoliation affects tassel branch number and tiller length, but not pistil size. a) *gt1;ra3* tassels of untreated and defoliated plants. b) Bases of *gt1;ra3* plants, arrow indicates main stalk, numbers indicate tillers. Tassel branching and tillering significance tested with a 2-way ANOVA assessing block and treatment effects. *** = p-value < .05. c) Pistil x-rays from *gt1;ra3* tassels. Significance tested with a mixed linear model: pistil area ~ treatment * block + (1 | plant). n.s. = not significant.

We grew B73 (WT), *gt1*, *ra3*, *tb1*, *tb1;ra3* and *tb1;gt1;ra3* mutants in the field and x-rayed tassel branches for analysis (Fig. 4a). *tb1;gt1;ra3* mutants had tassel-like ear inflorescences with silks

(Supplementary Fig. 4). After filtering out plants with tassels that had fewer than 5 detected pistils, only *gt1*, *gt1;ra3* and *tb1;gt1;ra3* plants remained. *gt1* pistils were smaller than both *gt1;ra3* and *tb1;gt1;ra3*; however *gt1;ra3* and *tb1;gt1;ra3* pistil sizes were not significantly different (Fig. 4b). *tb1*, *ra3* and *tb1;ra3* did not have visible pistils at maturity, as confirmed by scanning electron microscopy (SEM, Fig. 4c). Importantly, all detected pistils in *tb1;ra3* double mutants were

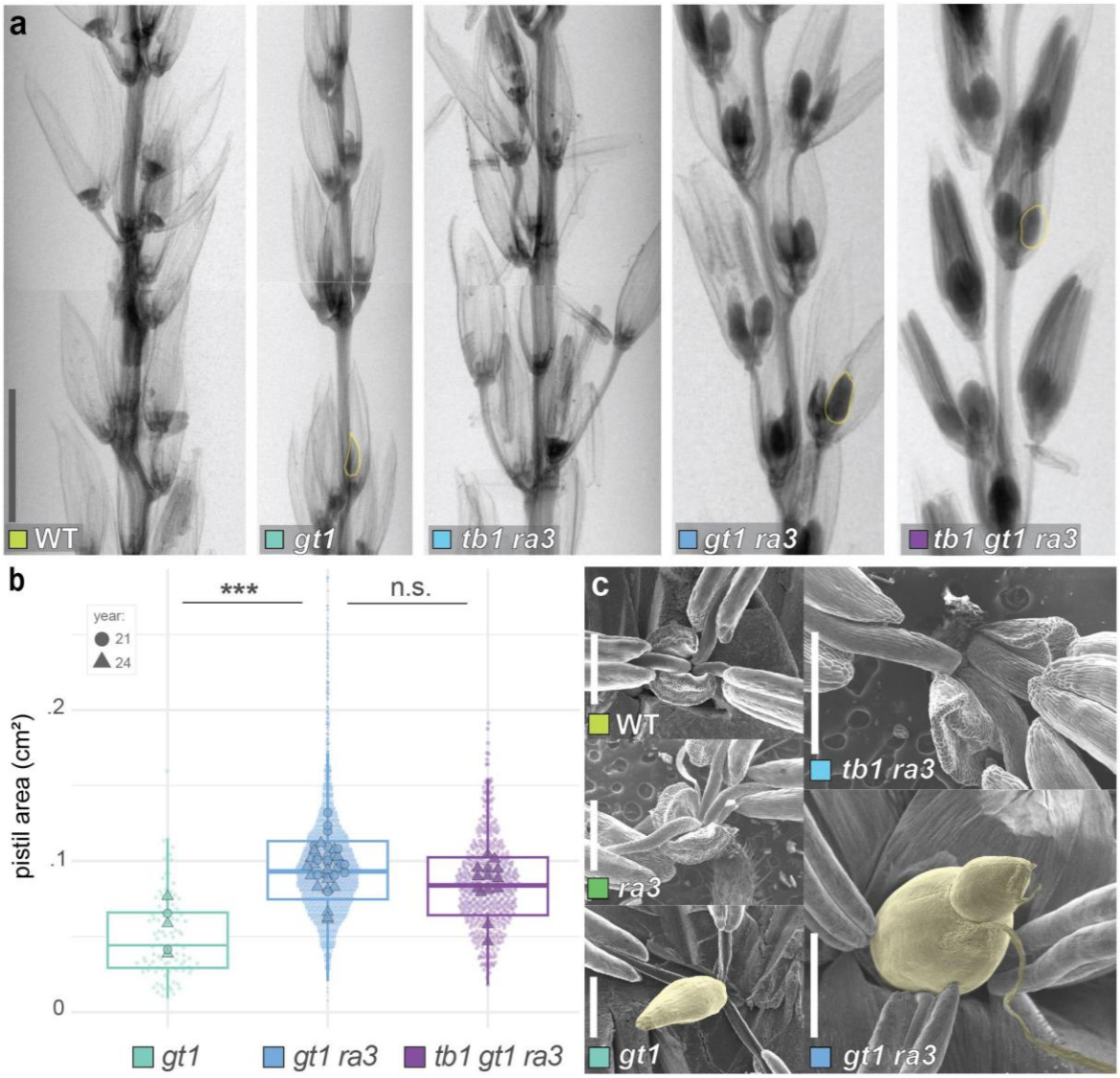

Figure 4. *tb1* does not affect pistil size in *ra3* or *gt1;ra3* backgrounds. a) X-ray tassel sections of WT (B73), *gt1*, *tb1;ra3*, *gt1;ra3*, and *tb1;gt1;ra3*. Example pistils are highlighted in yellow. b) Pistil area comparison between *gt1*, *gt1;ra3* and *tb1;gt1;ra3*. Additional plants were also included in this analysis (B73 - 9, *gt1* - 6, *tb1;ra3* - 2, *tb1* - 13, *ra3* - 2) however they all had less than 5 pistil detections per branch, which was considered the threshold for background noise, and were therefore filtered out. For statistical comparisons, a mixed linear model was used: pistil size ~ genotype * block + (1 | plant_id) with estimated marginal means. *** = $p < .05$; n.s. = not significant. c) SEM images of mature tassel florets from various genotypes. Pistils are highlighted with yellow.

individually evaluated and clearly represented false positives. Therefore, unlike in vegetative branching, *tb1* does not affect pistil size in *ra3* or *gt1;ra3* backgrounds. The absence of pistils in *tb1;ra3* mutants indicates that TB1 is unlikely to act upstream of *GT1* or *RA3* in tassel pistil suppression (Fig. 5). In addition, similar pistil sizes between *gt1;ra3* and *tb1;gt1;ra3* mutants indicates that TB1 is not suppressing pistil size through a separate pathway to *GT1* and *RA3.* This is distinct to tillering, where TB1 regulates both *GT1* and *TASSELS REPLACE UPPER EARS1 (Dong et al., 2017, 2019)*.

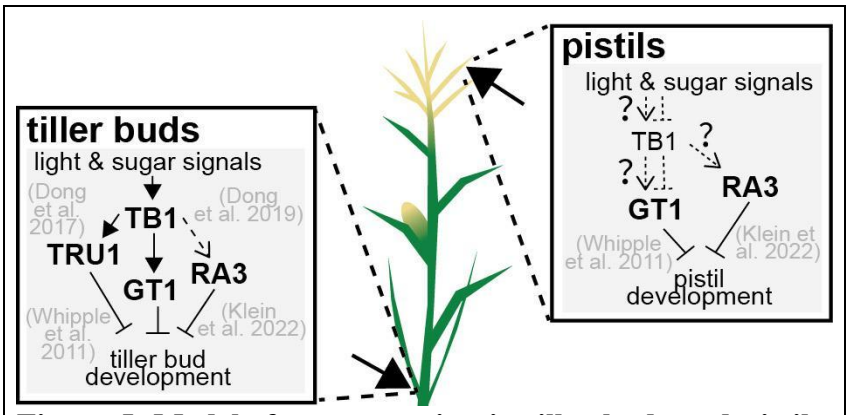

Figure 5. Models for suppression in tiller buds and pistils. Left) Tiller buds are suppressed by *GT1*, which is activated by TB1 in tiller buds in response to light and possibly sugar signals (Whipple *et al.*, 2011; Mason *et al.*, 2014). TB1 promotes the expression of *RA3* (Dong *et al.*, 2019). *RA3* with *GT1* suppresses tiller bud growth (Klein *et al.*, 2022). Right) Possible model for pistil suppression.

Discussion

Conserved developmental modules may have been redeployed in the evolution of pistil suppression, as some genes that suppress tiller growth also suppress pistil growth (Whipple *et al.*, 2011). To assess whether an axillary meristem suppression module had been recruited to pistil suppression in the evolution of grass flower morphology, we developed a method to precisely measure the size and shape of pistils in different conditions. Using this method, we found that defoliation, as a proxy for sugar deprivation (Kebrom *et al.*, 2010; Kebrom & Mullet, 2015) does not affect the size or shape of pistils in the tassel, even while it greatly reduces tillering and inflorescence branching. Through mutant comparisons, we determined that *GT1* is likely not downstream of TB1 in pistil suppression. These results indicate that tiller and pistil suppression mechanisms, while controlled by some of the same genes, have distinct upstream regulation.

Scientific progress is often limited by what one can observe; observational gaps can create bottlenecks in understanding plant phenotypes (Atkinson *et al.*, 2019). This especially applies to the study of pistil development in grasses because pistils need to be individually dissected out of tiny spikelets to be measured. Floral development, specifically the formation of pistils vs. stamens in unisexual flowers, is quantitative rather than binary (Lloyd, 1980; Pannell, 2017; Subramaniam & Bartlett, 2023), and the final form a flower takes can depend on several factors such as position (Diggle, 1995; Orr *et al.*, 2001), gene dosage (Moschin *et al.*, 2021), and environment (Lan *et al.*, 2023). These small quantitative differences in floral development are difficult to measure, especially in grasses. Our approach integrates x-ray imaging with machine learning-based

segmentation, making it feasible to measure multiple pistils simultaneously, and extract detailed data regarding their size, shape, and position. Trained across genotypes and species, our model captures features that generalize evolutionarily, extending its utility beyond maize to diverse grasses.

The ability to identify subtle phenotypic changes has broad application in biology, particularly in understanding complex plant traits and their evolution. The omnigenic model proposes that hundreds to thousands of genes influence a trait, but on their own genes may have very weak or no phenotype (Boyle *et al.*, 2017; Mähler *et al.*, 2020). In addition, complex dosage interactions amongst small-effect alleles may generate synergistic phenotypic outcomes (Zebell *et al.*, 2025). Accurately identifying minor phenotypic differences can help detect small-effect alleles, and reveal incremental genetic changes that underpin evolutionary processes and phenotypic diversity. Additionally, finding mutations that have weak effects on a trait can provide new variation for plant breeding programs (Muños *et al.*, 2011; Rodríguez-Leal *et al.*, 2017). While many new technologies can be expensive and inaccessible for labs (Rogers *et al.*, 2024), machine learning models are becoming increasingly accessible (Gehan *et al.*, 2017; Winfree, 2022). This work demonstrates how a fine-tuned computer vision model can be applied to a large image dataset to overcome phenotyping limitations and reveal new things about flower development.

Negative pleiotropy can be circumvented through *cis*-regulatory evolution, as mutations in regulatory elements of pleiotropic genes can restrict changes to a specific tissue and avoid harmful side effects (Carroll, 2008). Our results suggest that this mechanism of avoiding negative pleiotropy might increase the potential for developmental novelty when genes are redeployed across distinct developmental contexts, recruited by different upstream regulators. *GT1* is broadly capable of growth suppression, potentially through jasmonic acid signaling (Klein *et al.*, 2022; Yuan *et al.*, 2025). Supporting this generalizable function, ectopic expression of maize *GT1* in arabidopsis under a floral whorl-specific promoter reduced stamen and petal sizes (Gallagher *et al.*, 2023). Likewise, cis-regulatory changes upstream of *GT1* may drive its expression in tassel pistils, where it suppresses growth. Flexible regulatory mechanisms may allow unique roles for genes like *GT1* and *RA3* across developmental contexts, which then manifest as genetic pleiotropy in null mutants. In the grasses in particular, repeated recruitment of growth suppression genes may have led to floral diversification through the suppression of specific floral organs (Komatsuda *et al.*, 2007; Klein *et al.*, 2022; Gallagher *et al.*, 2023). In this case, recruitment of a growth suppression module may be a cause - not a consequence - of genetic pleiotropy.

Materials and Methods

Plant Material and Growth Conditions

We used the maize genotypes B73, *gt1-P* (Gallagher *et al.*, 2023), *ra3*, *tb1*, *tb1 ra3*, *gt1 ra3*, and *tb1 gt1 ra3* for phenotyping. We used the *gt1* allele *gt1-1* introgressed into B73 (Whipple *et al.*, 2011; Klein *et al.*, 2022). The *ra3* used was *ra3-fea1* (B73 background) (Satoh-Nagasawa *et al.*,

2006). The *tb1* allele used was *tb1-ref* introgressed into B73 (Doebley *et al.*, 1997). Maize was grown at the University of Massachusetts Amherst Crop and Animal Research and Education Farm in South Deerfield, MA (~42°290N, 72°350W) and setaria plants were grown at the College of Natural Sciences and Education Greenhouse on the UMass Amherst campus under long day conditions (16 h light, 8 h dark) at 28°C. Maize for defoliation experiments was grown at the University of Massachusetts Amherst Crop and Animal Research and Education Farm (~42°29′N, 72°35′W).

Defoliation Assay and Phenotyping

Plants were split across different parts of the field in a block design. Every other plant in the row was defoliated by removing half of the most recently exposed leaf starting at 3 weeks after planting and repeating every 3-4 days for 5 weeks. This experiment was repeated for 2 field seasons. Tiller length measurements were standardized to plant height and then averaged per plant.

X-ray Imaging

X-ray scans were captured using a Bruker Skyscan 1276 uCT at the Animal Imaging Core Facility on the UMass Amherst campus. Inflorescence samples were loaded horizontally into the machine. Samples were x-rayed from a reduced number of angles, and multiple scans were captured along the length of the sample. A single image angle from the top was selected and used in subsequent analyses. Scans were taken at 1008x672 resolution. The zoom level was set at 30µm per pixel for maize, and 40µm per pixel for setaria. All maize x-ray scans were taken at anthesis, and the bottommost tassel branch was used for imaging.

Pistil segmentation model

To train the model we first generated the training, validation and test data sets (table S1). Maize mutants with defects in tassel pistil repression were grown in either the field (UMass Amherst Crop and Animal Research and Education Farm) or the greenhouse (UMass Amherst College of Natural Sciences and Education Greenhouse). To obtain a range of pistil phenotypes, we grew the inbred line B73 as the negative control, *gt1-P*, *gt1 ra3* and *tb1 gt1 ra3* mutants. We also included *Setaria viridis* inflorescence examples to make the model more generalizable for pistil detection in other grass species. For these examples, we collected setaria at various growth stages to get a range of pistil sizes for training. Setaria x-rays were collected at 4 developmental stages (28, 31, 33, 42 days after sowing (DAS)). Branches were removed from the setaria inflorescences with tweezers to reduce overlap, and the thinned inflorescence was used for imaging. After obtaining x-ray images for all samples, we annotated pistils by tracing using the Via-annotator program (Dutta & Zisserman, 2019).

We used Roboflow (Dwyer, B., Nelson, J., Solawetz, J., et. al., 2022) to standardize the input image size in the case of different resolutions and to generate synthetic training examples using rotation (+- 10 degrees), brightness (+- 7%), and blur (up to .5px). The total dataset size was 332

tassel x-rays without synthetic data, and 664 after adding synthetic data. X-ray images were converted from tiff to jpg format, and pistil annotations were checked for accuracy in a Jupyter notebook (available on Github) before training.

Pistils in x-ray images are dense (20+ pistils per image) and overlapping. Because of this, Mask-RCNN (He *et al.*, 2017) was chosen as the base model due to its ability to segment overlapping objects effectively (Rettenberger *et al.*, 2023). Pistil-specific models were trained using Mask R-CNN with a ResNet-101-FPN backbone, pretrained on ImageNet and obtained from the Detectron2 Model Zoo (Yuxin Wu, Alexander Kirillov, Francisco Massa, Wan-Yen Lo, Ross Girshick, 2019). Models were trained using the Detectron2 framework using the default Mask-RCNN hyperparameter configurations. Training was completed on the Unity Cluster located at the Massachusetts Green High Performance Computing Center. During training several metrics were logged every 200 iterations, including total loss, validation loss, bounding box AP and segmentation AP. Model selection was based on the lowest validation loss. Checkpoints were saved every 200 iterations, and the final model was selected at iteration 1399 when validation loss plateaued.

We used stratified 5-fold cross-validation to evaluate model performance (table S2). Data splitting was implemented in Python using StratifiedKFold from scikit-learn, stratified by plant species (maize vs. setaria) and pistil size category (small, medium, large, extra-large). This ensured each fold contained a balanced composition of image types. For each fold, models were trained as described above, and training was stopped at 1399 iterations. Model performance across folds was assessed using bounding box and segmentation precision (AP) and consistency was compared across splits. The final model was evaluated using the hold-out test set with coco evaluation metrics (table S3). Lastly, a confidence threshold of 0.82 was applied to maximize the F1 score at high IoUs (fig. S1).

Pistil area and shape genotype comparison

Maize plants from all genotypes were grown for pistil area and shape quantification (see Plant Material and Growth Conditions). Tassel x-ray scans were collected as described above. The final pistil segmentation model with the 0.82 confidence threshold applied was used to generate pistil masks from the x-ray scans. First, pistil detections were filtered to remove detections of cut-off pistils at the edges of the image. Duplicate pistils in the regions where successive x-ray scans overlap were also removed. Tassels with less than 5 detections per tassel were filtered from the analysis. Pistil size was calculated from the total pixels in the detection mask. Pistil shape metrics were calculated using Python OpenCV. Fourier shape analysis was done using the program SHAPE (Iwata & Ukai, 2002). To quantify the pistil presence/absence by tassel branch position, model outputs were manually checked against the original x-rays to ensure no pistil detections were missed. To find pistil pairs within spikelets, a custom python script was used to identify instances where only two pistil masks overlapped. Any singletons or overlaps of more

than two pistils were discarded from the analysis. Identified pistil pairs were viewed to confirm pairs were correct before downstream analysis. All analyses were performed in Jupyter notebooks or R, and files are available on Github.

Genotyping Assays

tb1 ra3 and *tb1 gt1 ra3* plants were genotyped with the following primers:*tb1-ref* forward - GCCTTGGAGTCCCATCAGT, *tb1-ref* reverse - TTCATCGTCACACAGCCAAT; *ra3-fea1* forward CGGGAGGCGGGGAACTAATA, *ra3-fea1* reverse - AGTAGCACTCTGGGAAAGCG. A fragment surrounding the *tb1-ref* or *ra3-fea1* lesion was amplified with Phusion High-Fidelity DNA Polymerase (New England Biolabs) using the supplied HF buffer. Thermal cycling conditions were as follows: initial denaturation at 98 °C for 30 s; 30 cycles of 98 °C for 10 s, primer-specific annealing temperature (*tb1-ref* 63 °C, *ra3-fea1* 64 °C) for 20 s, and 72 °C for 30 s/kb; with a final extension at 72 °C for 5 min. PCR products were purified with the DNA Clean & Concentrator kit (Zymo Research) and submitted for Sanger sequencing.

Scanning Electron Microscopy (SEM)

SEM was performed with a JEOL JCM-6000 Plus Neoscope Benchtop scanning electron microscope with fresh tissue samples. Late-stage florets were dissected from the tassel and transferred to the SEM. Images were recorded under high vacuum and 5-kV voltage within 15 min of being in the SEM.

Acknowledgements: We thank D. Chitwood, C. Whipple, E. Kellogg, and A. Green for their helpful comments; I. Higgins for technical assistance; C. Joyner for plant care.

References:

Aguilar-Martínez JA, Poza-Carrión C, Cubas P. **2007**. Arabidopsis BRANCHED1 acts as an integrator of branching signals within axillary buds. *The Plant cell* **19**: 458–472.

Atkinson JA, Pound MP, Bennett MJ, Wells DM. **2019**. Uncovering the hidden half of plants using new advances in root phenotyping. *Current opinion in biotechnology* **55**: 1–8.

Barbier FF, Lunn JE, Beveridge CA. **2015a**. Ready, steady, go! A sugar hit starts the race to shoot branching. *Current opinion in plant biology* **25**: 39–45.

Barbier F, Péron T, Lecerf M, Perez-Garcia M-D, Barrière Q, Rolčík J, Boutet-Mercey S, Citerne S, Lemoine R, Porcheron B, *et al.* 2015b. Sucrose is an early modulator of the key hormonal mechanisms controlling bud outgrowth in Rosa hybrida. *Journal of experimental botany* **66**: 2569–2582.

Bertolini E, Rice BR, Braud M, Yang J, Hake S, Strable J, Lipka AE, Eveland AL. **2025**. Regulatory variation controlling architectural pleiotropy in maize. *Nature communications* **16**:

2140.

Boyle EA, Li YI, Pritchard JK. **2017**. An expanded view of complex traits: From polygenic to omnigenic. *Cell* **169**: 1177–1186.

Calderon-Urrea A, Dellaporta SL. **1999**. Cell death and cell protection genes determine the fate of pistils in maize. *Development* **126**: 435–441.

Carroll SB. **2005**. Evolution at two levels: on genes and form. *PLoS biology* **3**: e245.

Carroll SB. **2008**. Evo-devo and an expanding evolutionary synthesis: a genetic theory of morphological evolution. *Cell* **134**: 25–36.

Demotes-Mainard S, Péron T, Corot A, Bertheloot J, Le Gourrierec J, Pelleschi-Travier S, Crespel L, Morel P, Huché-Thélier, Lydie, Boumaza R, *et al.* 2016. Plant responses to red and far-red lights, applications in horticulture. *Environmental and experimental botany* **121**: 4–21.

Diggle P. **1995**. Architectural effects and the interpretation of patterns of fruit and seed development. *Annual Review of Ecology, Evolution, and Systematics* **26**: 531–552.

Diggle PK, Miller JS. **2004**. Architectural effects mimic floral sexual dimorphism in Solanum (Solanaceae). *American journal of botany* **91**: 2030–2040.

Dixon LE, Greenwood JR, Bencivenga S, Zhang P, Cockram J, Mellers G, Ramm K, Cavanagh C, Swain SM, Boden SA. **2018**. TEOSINTE BRANCHED1 regulates inflorescence architecture and development in bread wheat (Triticum aestivum). *The plant cell* **30**: 563–581.

Doebley J, Stec A, Gustus C. **1995**. teosinte branched1 and the origin of maize: evidence for epistasis and the evolution of dominance. *Genetics* **141**: 333–346.

Doebley J, Stec A, Hubbard L. **1997**. The evolution of apical dominance in maize. *Nature* **386**: 485–488.

Dong Z, Li W, Unger-Wallace E, Yang J, Vollbrecht E, Chuck G. **2017**. Ideal crop plant architecture is mediated by tassels replace upper ears1, a BTB/POZ ankyrin repeat gene directly targeted by TEOSINTE BRANCHED1. *Proceedings of the National Academy of Sciences of the United States of America* **114**: E8656–E8664.

Dong Z, Xiao Y, Govindarajulu R, Feil R, Siddoway ML, Nielsen T, Lunn JE, Hawkins J, Whipple C, Chuck G. **2019**. The regulatory landscape of a core maize domestication module controlling bud dormancy and growth repression. *Nature communications* **10**: 3810.

Doust AN. **2007**. Grass architecture: genetic and environmental control of branching. *Current opinion in plant biology* **10**: 21–25.

Dutta A, Zisserman A. **2019**. The VIA Annotation Software for Images, Audio and Video. *arXiv [cs.CV]*.

Dwyer, B., Nelson, J., Solawetz, J., et. al. 2022. Roboflow (Version 1.0) [Software].

Egger RL, Walbot V. **2015**. Quantifying Zea mays L tassel development and correlation with anther developmental stages as a guide for experimental studies.

Fichtner F, Barbier FF, Annunziata MG, Feil R, Olas JJ, Mueller-Roeber B, Stitt M, Beveridge CA, Lunn JE. **2021**. Regulation of shoot branching in arabidopsis by trehalose 6-phosphate. *The New phytologist* **229**: 2135–2151.

Fichtner F, Barbier FF, Feil R, Watanabe M, Annunziata MG, Chabikwa TG, Höfgen R, Stitt M, Beveridge CA, Lunn JE. **2017**. Trehalose 6-phosphate is involved in triggering axillary bud outgrowth in garden pea (Pisum sativum L.). *The Plant journal: for cell and molecular biology* **92**: 611–623.

Foster KR, Shaulsky G, Strassmann JE, Queller DC, Thompson CRL. **2004**. Pleiotropy as a mechanism to stabilize cooperation. *Nature* **431**: 693–696.

Gallagher JP, Man J, Chiaramida A, Rozza IK, Patterson EL, Powell MM, Schrager-Lavelle A, Multani DS, Meeley RB, Bartlett ME. **2023**. *GRASSY TILLERS1* (*GT1*) and *SIX-ROWED SPIKE1* (*VRS1*) homologs share conserved roles in growth repression. *Proceedings of the National Academy of Sciences of the United States of America* **120**: e2311961120.

Gehan MA, Fahlgren N, Abbasi A, Berry JC, Callen ST, Chavez L, Doust AN, Feldman MJ, Gilbert KB, Hodge JG, *et al.* 2017. PlantCV v2: Image analysis software for high-throughput plant phenotyping. *PeerJ* **5**: e4088.

González-Grandío E, Pajoro A, Franco-Zorrilla JM, Tarancón C, Immink RGH, Cubas P. **2017**. Abscisic acid signaling is controlled by a BRANCHED1/HD-ZIP I cascade in Arabidopsis axillary buds. *Proceedings of the National Academy of Sciences of the United States of America* **114**: E245–E254.

González-Grandío E, Poza-Carrión C, Sorzano COS, Cubas P. **2013**. BRANCHED1 promotes axillary bud dormancy in response to shade in Arabidopsis. *The plant cell* **25**: 834–850.

Gross-Hardt R, Lenhard M, Laux T. **2002**. WUSCHEL signaling functions in interregional communication during Arabidopsis ovule development. *Genes & development* **16**: 1129–1138.

Gustin JL, Boehlein SK, Shaw JR, Junior W, Settles AM, Webster A, Tracy WF, Hannah LC. **2018**. Ovary abortion is prevalent in diverse maize inbred lines and is under genetic control. *Scientific reports* **8**: 13032.

Hämälä T, Gorton AJ, Moeller DA, Tiffin P. **2020**. Pleiotropy facilitates local adaptation to distant optima in common ragweed (Ambrosia artemisiifolia). *PLoS genetics* **16**: e1008707.

He K, Gkioxari G, Dollár P, Girshick R. **2017**. Mask R-CNN. *arXiv [cs.CV]*.

Hubbard L, McSteen P, Doebley J, Hake S. **2002**. Expression patterns and mutant phenotype of teosinte branched1 correlate with growth suppression in maize and teosinte. *Genetics* **162**:

1927–1935.

Iwata H, Ukai Y. **2002**. SHAPE: a computer program package for quantitative evaluation of biological shapes based on elliptic Fourier descriptors. *The journal of heredity* **93**: 384–385.

Jiao Y, Lee YK, Gladman N, Chopra R, Christensen SA, Regulski M, Burow G, Hayes C, Burke J, Ware D, *et al.* 2018. MSD1 regulates pedicellate spikelet fertility in sorghum through the jasmonic acid pathway. *Nature communications* **9**: 822.

Johnston R, Wang M, Sun Q, Sylvester AW, Hake S, Scanlon MJ. **2014**. Transcriptomic analyses indicate that maize ligule development recapitulates gene expression patterns that occur during lateral organ initiation. *The plant cell* **26**: 4718–4732.

Kebrom TH, Brutnell TP, Finlayson SA. **2010**. Suppression of sorghum axillary bud outgrowth by shade, phyB and defoliation signalling pathways. *Plant, cell & environment* **33**: 48–58.

Kebrom TH, Burson BL, Finlayson SA. **2006**. Phytochrome B represses Teosinte Branched1 expression and induces sorghum axillary bud outgrowth in response to light signals. *Plant physiology* **140**: 1109–1117.

Kebrom TH, Mullet JE. **2015**. Photosynthetic leaf area modulates tiller bud outgrowth in sorghum. *Plant, cell & environment* **38**: 1471–1478.

Khangura R, Johal GGS, Dilkes BP. **2020**. Variation in maize chlorophyll biosynthesis alters plant architecture. *Plant physiology*.

King MC, Wilson AC. **1975**. Evolution at two levels in humans and chimpanzees: Their macromolecules are so alike that regulatory mutations may account for their biological differences. *Science (New York, N.Y.)* **188**: 107–116.

Klein H, Gallagher J, Demesa-Arevalo E, Abraham-Juárez MJ, Heeney M, Feil R, Lunn JE, Xiao Y, Chuck G, Whipple C, *et al.* 2022. Recruitment of an ancient branching program to suppress carpel development in maize flowers. *Proceedings of the National Academy of Sciences of the United States of America* **119**.

Komatsuda T, Pourkheirandish M, He C, Azhaguvel P, Kanamori H, Perovic D, Stein N, Graner A, Wicker T, Tagiri A, *et al.* 2007. Six-rowed barley originated from a mutation in a homeodomain-leucine zipper I-class homeobox gene. *Proceedings of the National Academy of Sciences of the United States of America* **104**: 1424–1429.

Kostyun JL, Gibson MJS, King CM, Moyle LC. **2019**. A simple genetic architecture and low constraint allow rapid floral evolution in a diverse and recently radiating plant genus. *The new phytologist* **223**: 1009–1022.

Kumar V, Kim SH, Adnan MR, Heo J, Jeong JH, Priatama RA, Lee JJ, Kim CM, Je BI, Park SJ, *et al.* 2021. Tiller outgrowth in rice (Oryza sativa L.) is controlled by OsGT1, which acts downstream of FC1 in a PhyB-independent manner. *Journal of Plant Biology* **64**: 417–430.

Lan J, Wang N, Wang Y, Jiang Y, Yu H, Cao X, Qin G. **2023**. Arabidopsis TCP4 transcription factor inhibits high temperature-induced homeotic conversion of ovules. *Nature communications* **14**: 5673.

Le Roux LG, Kellogg EA. **1999**. Floral development and the formation of unisexual spikelets in the Andropogoneae (Poaceae). *American journal of botany* **86**: 354–366.

Lloyd DG. **1980**. The distributions of gender in four angiosperm species illustrating two evolutionary pathways to dioecy. *Evolution; international journal of organic evolution* **34**: 123.

Luo D, Carpenter R, Vincent C, Copsey L, Coen E. **1996**. Origin of floral asymmetry in Antirrhinum. *Nature* **383**: 794–799.

Luo Z, Janssen BJ, Snowden KC. **2021**. The molecular and genetic regulation of shoot branching. *Plant physiology* **187**: 1033–1044.

Mähler N, Schiffthaler B, Robinson KM, Terebieniec BK, Vučak M, Mannapperuma C, Bailey MES, Jansson S, Hvidsten TR, Street NR. **2020**. Leaf shape in Populus tremula is a complex, omnigenic trait. *Ecology and evolution* **10**: 11922–11940.

Martín-Trillo M, Grandío EG, Serra F, Marcel F, Rodríguez-Buey ML, Schmitz G, Theres K, Bendahmane A, Dopazo H, Cubas P. **2011**. Role of tomato BRANCHED1-like genes in the control of shoot branching: A BRC1-like gene controls shoot branching in tomato. *The Plant journal: for cell and molecular biology* **67**: 701–714.

Mason MG, Ross JJ, Babst BA, Wienclaw BN, Beveridge CA. **2014**. Sugar demand, not auxin, is the initial regulator of apical dominance. *Proceedings of the National Academy of Sciences of the United States of America* **111**: 6092–6097.

Miller JS, Diggle PK. **2003**. Diversification of andromonoecy in Solanum section Lasiocarpa (Solanaceae): the roles of phenotypic plasticity and architecture. *American journal of botany* **90**: 707–715.

Moschin S, Nigris S, Ezquer I, Masiero S, Cagnin S, Cortese E, Colombo L, Casadoro G, Baldan B. **2021**. Expression and functional analyses of Nymphaea caerulea MADS-box genes contribute to clarify the complex flower patterning of water lilies. *Frontiers in plant science* **12**: 730270.

Muños S, Ranc N, Botton E, Bérard A, Rolland S, Duffé P, Carretero Y, Le Paslier M-C, Delalande C, Bouzayen M, *et al.* 2011. Increase in tomato locule number is controlled by two single-nucleotide polymorphisms located near WUSCHEL. *Plant physiology* **156**: 2244–2254.

Nuccio ML, Wu J, Mowers R, Zhou H-P, Meghji M, Primavesi LF, Paul MJ, Chen X, Gao Y, Haque E, *et al.* 2015. Expression of trehalose-6-phosphate phosphatase in maize ears improves yield in well-watered and drought conditions. *Nature biotechnology* **33**: 862–869.

Orr HA. **2000**. Adaptation and the cost of complexity. *Evolution; international journal of organic evolution* **54**: 13–20.

Orr AR, Kaparthi R, Dewald CL, Sundberg MD. **2001**. Analysis of inflorescence organogenesis in eastern gamagrass, Tripsacum dactyloides (Poaceae): the wild type and the gynomonoecious gsf1 mutant. *American journal of botany* **88**: 363–381.

Pannell JR. **2017**. Plant sex determination. *Current biology: CB* **27**: R191–R197.

Patil SB, Barbier FF, Zhao J, Zafar SA, Uzair M, Sun Y, Fang J, Perez-Garcia M-D, Bertheloot J, Sakr S, *et al.* 2022. Sucrose promotes D53 accumulation and tillering in rice. *The new phytologist* **234**: 122–136.

Prud'homme B, Gompel N, Carroll SB. **2007**. Emerging principles of regulatory evolution. *Proceedings of the National Academy of Sciences of the United States of America* **104 Suppl 1**: 8605–8612.

Qian D, Wang M, Niu Y, Yang Y, Xiang Y. **2025**. Sexual reproduction in plants under high temperature and drought stress. *Cell reports* **44**: 115390.

Rainio O, Teuho J, Klén R. **2024**. Evaluation metrics and statistical tests for machine learning. *Scientific reports* **14**: 6086.

Rameau C, Bertheloot J, Leduc N, Andrieu B, Foucher F, Sakr S. **2014**. Multiple pathways regulate shoot branching. *Frontiers in plant science* **5**: 741.

Rettenberger L, Rieken Münke F, Bruch R, Reischl M. **2023**. Mask R-CNN outperforms U-Net in instance segmentation for overlapping cells. *Current directions in biomedical engineering* **9**: 335–338.

Rodríguez-Leal D, Lemmon ZH, Man J, Bartlett ME, Lippman ZB. **2017**. Engineering Quantitative Trait Variation for Crop Improvement by Genome Editing. *Cell* **171**: 470–480.e8.

Rogers CD, Amemiya C, Arur S, Babonis L, Barresi M, Bartlett M, Behringer R, Benham-Pyle B, Bergmann D, Blackman B, *et al.* 2024. Pluripotency of a founding field: rebranding developmental biology. *Development (Cambridge, England)* **151**: dev202342.

Rudall PJ. **1997**. The Nucellus and Chalaza in monocotyledons: Structure and systematics. *The Botanical review; interpreting botanical progress* **63**: 140–181.

Sánchez-Gerschon V, Martínez-Fernández I, González-Bermúdez MR, de la Hoz-Rodríguez S, González FV, Lozano-Juste J, Ferrándiz C, Balanzà V. **2024**. Transcription factors HB21/40/53 trigger inflorescence arrest through abscisic acid accumulation at the end of flowering. *Plant physiology* **195**: 2743–2756.

Satoh-Nagasawa N, Nagasawa N, Malcomber S, Sakai H, Jackson D. **2006**. A trehalose metabolic enzyme controls inflorescence architecture in maize. *Nature* **441**: 227–230.

Setter TL, Flannigan BA, Melkonian J. **2001**. Loss of kernel set due to water deficit and shade in maize: Carbohydrate supplies, abscisic acid, and cytokinins. *Crop science* **41**: 1530–1540.

Stearns FW. **2010**. One hundred years of pleiotropy: a retrospective. *Genetics* **186**: 767–773.

Subramaniam B, Bartlett M. **2023**. Re-imagining reproduction: The queer possibilities of plants. *Integrative and comparative biology* **63**: 946–959.

Takeda T, Suwa Y, Suzuki M, Kitano H, Ueguchi-Tanaka M, Ashikari M, Matsuoka M, Ueguchi C. **2003**. The OsTB1 gene negatively regulates lateral branching in rice. *The Plant journal: for cell and molecular biology* **33**: 513–520.

Tetio-Kagho F, Gardner FP. **1988**. Responses of maize to plant population density. I. canopy development, light relationships, and vegetative growth. *Agronomy journal* **80**: 930–935.

Welch JJ, Waxman D. **2003**. Modularity and the cost of complexity. *Evolution; international journal of organic evolution* **57**: 1723–1734.

Whipple CJ, Kebrom TH, Weber AL, Yang F, Hall D, Meeley R, Schmidt R, Doebley J, Brutnell TP, Jackson DP. **2011**. grassy tillers1 promotes apical dominance in maize and responds to shade signals in the grasses. *Proceedings of the National Academy of Sciences of the United States of America* **108**: E506–12.

Winfree S. **2022**. User-accessible machine learning approaches for cell segmentation and analysis in tissue. *Frontiers in physiology* **13**: 833333.

Yang H, Nukunya K, Ding Q, Thompson BE. **2022**. Tissue-specific transcriptomics reveal functional differences in floral development. *Plant physiology* **188**: 1158–1173.

Yant L, Collani S, Puzey J, Levy C, Kramer EM. **2015**. Molecular basis for three-dimensional elaboration of the Aquilegia petal spur. *Proceedings. Biological sciences* **282**: 20142778.

Yuan Y, Ou X, Yao M, Wang P, Li C, Zhang G, He M, Li H, Xu X, Zhong Z, *et al.* 2025. GT1 and ZmHB13/VRL1 regulate flower sexual differentiation by modulating jasmonate biosynthesis and signaling in maize. *Plant physiology* **197**: kiaf075.

Yuxin Wu, Alexander Kirillov, Francisco Massa, Wan-Yen Lo, Ross Girshick. **2019**. Detectron2.

Zebell SG, Martí-Gómez C, Fitzgerald B, Cunha CP, Lach M, Seman BM, Hendelman A, Sretenovic S, Qi Y, Bartlett M, *et al.* 2025. Cryptic variation fuels plant phenotypic change through hierarchical epistasis. *Nature* **644**: 984–992.

Zhang J. **2023**. Patterns and evolutionary consequences of pleiotropy. *Annual review of ecology, evolution, and systematics* **54**: 1–19.